Published in final edited form as:
J Biomed Mater Res A. 2015 January ; 103(1): 211–223. doi:10.1002/jbm.a.35165.

Direct *In Vivo* Inflammatory Cell-Induced Corrosion of CoCrMo Alloy Orthopedic Implant Surfaces

Jeremy L. Gilbert[1,2,*], **Shiril Sivan**[1,2], **Yangping Liu**[1,2], **Sevi Kocagöz**[3], **Christina Arnholt**[3], and **Steven M. Kurtz**[3,4]

[1]Syracuse Biomaterials Institute, Syracuse University, Syracuse NY 13244

[2]Department of Biomedical and Chemical Engineering, Syracuse University, Syracuse NY 13244

[3]School of Biomedical Engineering, Science, and Health Systems, Drexel University, Phildelphia, PA 19104

[4]Exponent, Inc, Phildelphia, PA 19104

Abstract

Cobalt-chromium-molybdenum alloy, used for over four decades in orthopedic implants, may corrode and release wear debris into the body during use. These degradation products may stimulate immune and inflammatory responses in vivo. We report here on evidence of direct inflammatory cell-induced corrosion of human implanted and retrieved CoCrMo implant surfaces. Corrosion morphology on CoCrMo implant surfaces, in unique and characteristic patterns, and the presence of cellular remnants and biological materials intimately entwined with the corrosion indicates direct cellular attack under the cell membrane region of adhered and/or migrating inflammatory cells. Evidence supports a Fenton-like reaction mechanism driving corrosion in which reactive oxygen species are the major driver of corrosion. Using in vitro tests, large increases in corrosion susceptibility of CoCrMo were seen (40 to 100 fold) when immersed in phosphate buffered saline solutions modified with hydrogen peroxide and HCl to represent the chemistry under inflammatory cells. This discovery raises significant new questions about the clinical consequences of such corrosion interactions, the role of patient inflammatory reactions, and the detailed mechanisms at play.

1. Introduction

Cobalt-chromium-molybdenum alloy (CoCrMo, ASTM F-75, F-*1537*[1,2]) is one of the most widely used metals in implants for the repair, replacement, or augmentation of the human body. This metallic biomaterial has been in use since the late 1920's, first as a dental alloy and later as a metallic biomaterial for orthopedic, spinal and cardiovascular implant applications. Recently, there have been concerns raised about the effects of ions and particles released from CoCrMo-based orthopedic implants on the body's response. Pseudotumors[3,4] (non-cancerous fluid filled cysts), adverse reaction to metal debris (ARMD)[5,6] and adverse local tissue reactions (ALTR)[7,8] are phrases used currently by

*Corresponding Author, gilbert@syr.edu.

clinicians and researchers to describe the potential effects of metallic wear and corrosion damage on the local biological system.

Mechanically assisted corrosion mechanisms, also referred to as tribocorrosion[9–12], present at bearing surfaces and within modular taper connections between components of the arthroplasty device, have been thought to be the primary processes by which ions and particles are generated in the implant-body system. Increased incidence and severity of biologically-based reactions to these corrosion products have been reported recently with the increased use of total hip and total knee replacements. It is clear that there is an inflammatory and/or immune response that arises in some patients as a result of adverse reactions to metal debris[13–15], and the processes of mechanically assisted corrosion[16,17] present in these devices. That is, the body sometimes responds to these implant damage-generating mechanisms by activating the immune and/or inflammatory systems of the body. It is not clear why some patients respond to the presence of elevated exposure to metal debris, while others do not.

Here, we present new evidence of direct inflammatory cell induced (ICI) corrosion of CoCrMo alloy implant surfaces from microscopic observations of previously implanted and subsequently retrieved hip and knee implants. The cells thought to be engaged in this direct attack are the class of cells collectively known as inflammatory cells or phagocytic cells in the skeletal system that include osteoclasts, macrophages, foreign body giant cells and potentially others (polymorphonuclear leucocytes, etc.). Which of these cell types are involved, and in what proportion, is not known. However, we present evidence of corrosion that directly results from attack under the cell membrane and which exhibits unique cell-derived morphologies and which have biological material and/or cellular remnants intimately attached to the corroded regions. Unique and characteristic patterns are seen in non-contact regions of articular surfaces (i.e., regions that are part of the polished bearing surface, but which do not make contact with the opposing tribological surface, e.g., distal region of the head), and non-articular machined surfaces of retrieved CoCrMo implants. Additionally, the effect of reactive oxygen species (ROS), specifically hydrogen peroxide, on the corrosion susceptibility of CoCrMo is measured in vitro to demonstrate ROS chemistry, similar to that reported to occur under a phagocytic cell's ruffled border region (i.e., H_2O_2, HCl), significantly increases the corrosion susceptibility of CoCrMo.

2. Materials and Methods

2.1. Experimental Methods for Retrieval Analyses

Retrieved implants analyzed in this study came from two sources. First, implants were obtained from the NIH funded Implant Retrieval Center at Drexel University. Participating surgeons from 14 different centers provided both hip and knee implants from a range of companies. A second source came from a corporate-funded research program at Syracuse University which consisted of hip replacements that were of a metal-on-metal bearing design. Only a subset of implants in the Drexel retrieval program (of which there are currently over 4,600 total hip and knee implants) were analyzed. The components reported on here were selected based on obvious corrosion in the modular taper regions of these devices in order to study taper corrosion modes in these devices. The ICI corrosion reported

on here was serendipitously observed in the course of the taper study and were seen in regions remote from the tapers.

The implants received by the Drexel retrieval program were cleaned by water rinsing followed by sterilization using a 5% NaOCl solution. Devices obtained from the implant manufacturer were steam sterilized. Neither process resulted in significant corrosion damage or alteration of CoCrMo surfaces. Steam sterilization did not completely eliminate evidence of biological materials or cell remnants on the surfaces and thus were able to be captured.

Devices were catalogued and any patient-specific information was de-identified as per IRB protocol. General information concerning time of implantation, reason for revision, etc. when available, was cataloged, however, the intent of this work was not focused on clinical variables, but rather just documentation and characterization of the phenomenon, and on what implant types it was observed.

A total of 69 different CoCrMo retrieved components from 51 implant systems were investigated (19 from SU and 32 from Drexel) including 18 hip acetabular liners, 37 heads and 14 knees. The retrieved implants studied here are hip and knee implants spanning over 0.1 to 17.9 years of implantation time. A range of designs (hip and knee), bearing combinations and CoCrMo alloy types were investigated. Bearing combinations include CoCrMo on CoCrMo (so-called metal-on-metal, MOM) articulations, and metal on ultra-high molecular weight polyethylene (UHMWPE), so called metal-on-polymer (MOP) articulations. The CoCrMo alloys observed in retrievals were both cast (ASTM F-75, *(1)*) and wrought alloys (ASTM F-1537, *(2)*). The reasons given for implant retrieval were categorized. However, no attempt was made to correlate inflammatory cell induced corrosion and reasons for revision.

ICI corrosion was identified on articulating surfaces (polished regions) and on non-articulating surfaces. On articulating surfaces, the corrosion was seen in regions that are not engaged in bearing interactions with the opposing surface. This includes, for example, the hip head polished surface around the perimeter (i.e., outside of the contact zone), the peripheral femoral condyle of the knees in the posterior-lateral (or medial) regions, and on the rim of the metal acetabular components and just inside the rim on the articulating surface. Non-articular surfaces included the machined surfaces of the femoral head between the taper junction and the articular surface, the superior shoulder of a CoCrMo femoral stem and on the neck outside of the taper, and on the machined surfaces of the metal acetabular liners.

2.2. Imaging and Retrieval Analysis

Devices were analyzed with both optical and scanning electron microscopy (SEM) methods. For optical microscopy, a digital optical microscope (Hirox 8700, Hirox, Inc. Mahwah, NJ) was used. This system provides infinite focus three dimensional imaging capabilities, along with montage capabilities. A range of magnifications were explored from roughly 30X to 3000X. No additional cleaning methods were used for most analyses. In one case, a cotton swab with water and then ethanol was used to rub the corroded region to determine if the patterns were due to adhered biological debris, but no change was observed as a result.

Scanning electron microscopy (JEOL 5600, JEOL, USA, Dearborn MA) with energy dispersive spectroscopy (EDS, Princeton Gamma Tech, Princeton, NJ) was used. The SEM imaging methods included both secondary (SEI) and backscattered (BEC) electron imaging. Both high accelerating voltage (kV, 10 to 15 kV) and low kV (2 to 4 kV) SEI imaging was used. Low kV imaging of non-conducting biological materials provides significantly enhanced ability to image cellular membranes and biological materials on the surfaces of CoCrMo. Lower energy electron beams do not penetrate cell membranes and reveal biological materials preferentially, whereas high energy electron beams will pass mostly through cell membranes and biological materials with few scattered electrons providing image contrast. High kV SEI provides topographic information of the alloy and corroded surfaces, while high kV BEC provides both topographic and compositional information concerning the surface including carbide and oxide identification as well as biological materials. EDS was used to characterize the elements present in selective regions by focusing the electron beam on the region of interest and capturing the characteristics x-rays emanating from the sample. A range of accelerating voltages (10kV to 15 kV) was used, with 15 kV typical for EDS analysis. No special sample preparation was used beyond the initial cleaning and sterilization methods.

2.3. Simulated In Vitro Corrosion Testing of CoCrMo in H_2O_2 containing physiological solutions

Corrosion test methods used to assess CoCrMo susceptibility to in vitro corrosion in physiological solutions modified with acid and/or hydrogen peroxide included monitoring of Open Circuit Potential (OCP), capture of the voltage versus log of the current density (polarization testing), and measuring the impedance of the interface as a function of frequency of the oscillating voltage superimposed over the resting OCP.

CoCrMo (ASTM F-1537) disks were obtained from an orthopedic manufacturer. These disks were prepared for corrosion testing by polishing through a series of grits to 600 grit with wet emery paper. Samples were mounted in a corrosion test cell that provided exposure of about 4 cm^2 of metal surface. A potentiostat (Solatron 1380) was used for all electrochemical testing with software for control and acquisition of electrochemical signals (Zcorr, and Zview, Schribner and Associates).

A three electrode electrochemical cell was used wherein the reference electrode was a saturated silver-silver chloride (Ag/AgCl) reference electrode (0.222 V vs NHE) and the counter electrode was a carbon rod.

The solutions used were room temperature phosphate buffered saline (PBS, Sigma) made with distilled water. Additions of hydrochloric acid (HCl) and hydrogen peroxide (H_2O_2) were made to cover a range of pH's (1, 3 and 7.4) and H_2O_2 concentrations (from 0.1 mM to 30 mM).

OCP vs Time—The OCP of CoCrMo disks was monitored for at least ½ hour for each solution tested. For H_2O_2 tests, the H_2O_2 was added after the start of testing to show where a distinct change in voltage occurs due to the introduction of H_2O_2. HCl was added to adjust the pH which was monitored using a pH meter. Each test was repeated three times.

Polarization Tests—In these tests, CoCrMo samples in various PBS solutions adjusted with H_2O_2 and HCl were performed. Here, the samples were started at −1 V and scanned anodically at 1 mV/s to +1 V. Tests across a range of pH's and H_2O_2 concentrations were performed. Each condition was repeat tested on a freshly polished sample three times.

Impedance Analysis—Electrochemical impedance spectroscopy was performed by first allowing the CoCrMo sample to come to an equilibrium OCP (after 1 h) in the test solution (PBS, or PBS with H2O2 and/or HCl, as described above) and then the sample was fixed at that potential and a 10 mV sinusoidal voltage was superimposed on the static OCP. The frequency of oscillation was between 20 kHz and 0.01 Hz and the phase angle and impedance magnitude was captured. Three samples per solution condition were tested. Low frequency impedance (at 0.01 Hz), which reflects the surface oxide resistance was used for comparisons of surface behavior.

In all results, only representative plots are presented, however, the behavior observed was consistent across repeated testing for all experiments.

3. Results

3.1. Inflammatory Cell Induced Corrosion In Vivo

Of the 69 different CoCrMo retrieved components from 51 implant systems, inflammatory cell induced corrosion was seen in 51 different components. The reasons for revision for each implant type (Table 1) include infection, pain, loosening and ALTR and several others. Each implant type has a different distribution of reasons given for revision with more infections for the knees, loosening for MOP hips and pain and ALTR for the MOM hips.

Examples of ICI corrosion (Figure 1) are shown at low magnification in digital optical microscopic images as light frosted or discolored areas on the implant surface (Fig. 1A). Higher magnification optical images reveal these frosted regions to consist of fine pits and streaks, and zones of attack (Fig. 1B). The range of characteristic features of the ICI corrosion can be seen (Fig. 1C to 1F). These include individual spots of apparently discolored regions (consisting of a ruffled topography) with small pits or circular or irregular crater-like features (Fig. 1E and 1F), as well as larger more generally hazy surfaces (Fig. 1C and 1D). The corrosion damage in Fig. 1C is taking place on a knee prosthesis on the posterior condylar surface of the cast CoCrMo alloy (carbides are visible on the center-right of the image). The bearing counter surface for the knee was polyethylene as it was for the hip in Fig. 1B and 1F (MOM bearing surfaces are shown in Fig. 1D and 1E). The dimensions of the damaged regions vary, but when a single cell damage site is observed (see arrows in Fig. 1E and 1F) there are typically darker halo regions consisting of a ruffled topography, with one to three or more crater-like features present. This is a highly consistent appearance across all components investigated.

The following results discuss several examples of evidence of inflammatory cell induced corrosion arising from a cell or cells migrating across the implant surface. The first example, Fig. 2, is of the non-contact region of the articular surface of the head of a MOM couple, near the perimeter of the polished region. Low magnification imaging (Fig. 2A) of the ICI

region shows the polished edge (on left) and several hazy corrosion patterns (upper right) and a roughly vertical line in the middle of the image. This line is a corrosion streak left by a transiting cell as it migrated over the surface. A higher magnification DOM micrograph (Fig. 2B) shows the same line as in Fig. 2A and the white arrow in each figure points to the same location. The line is made up of pits and wavy lines of corrosion processes. The pits are small, on the order of 10 um or smaller, and the line is somewhat wavy. The left-most patch in Fig. 2B (see black arrow) is imaged with SEM in Figs. 2C–2E in the three imaging modes (low kV SEI, Fig. 2C, high kV SEI, Fig. 2D, and high kV BEC, Fig. 2E). The low kV SEI (Fig. 2C) image reveals biological materials (bright contrast) inside the corroded regions, whereas the two high kV images show more of the topography of the surface. The bright regions were also evaluated with EDS and were found to have high carbon concentrations consistent with biological materials (along with other elements). The examples in Fig. 2F–2H, and 2I–2J are higher magnification sets of the line of corrosion using the three imaging modes. These examples show more clearly the relationship between the biological materials (bright in Fig. 2F and 2I), with the topography and alloy chemistry seen in Figs. 2G–H and 2J–K, respectively. It is interesting to see how the bright cellular material seen at low kV is reduced significantly in the higher kV images. The biological material resides inside corrosion pits or surround the topographic features of the corroded CoCrMo.

Examples of the corrosion patterns of other migrating cells are presented in the DOM micrographs of Figure 3. In these images, the cell attached to an initial site (see arrow in Fig. 3A), and then proceeded to engage in attack of the substrate alloy with a repeated advancing front seen as progressive circular arcs of damage. The cell causing the corrosion seen in Fig. 3A was attacking the head of a MOP hip implant on the articulating surface (outside the bearing zone) and first progressed toward the lower left, and then changed directions and moved upward and expanded its front of attack. Additional images (Fig. 3B to 3D) are from MOM heads and show similar behavior.

This corrosion pattern was seen numerous times (n>10) in our investigation. The advancing front repeats a pattern of alternating ruffled and smooth regions which, when imaged in the SEM (Fig. 4) show the detailed pattern of attack. Figure 4 shows two matched pairs of high kV SEI and BEC images detailing the fine biologically-derived corrosion patterns seen in Fig. 3. The high kV SEI images (Fig. 4A and 4C) highlight topography of the corroded CoCrMo and the backscattered images (Fig. 4B and 4D) reveal the underlying microstructure of the CoCrMo alloy which contains blocky carbides (dark particles) and Mo-Si-O particles, (bright spots in the image) and the interaction of the ICI attack with the microstructure. The features of the attack are consistent across all implants seen with this form of corrosion. The fine micron-scale pattern suggests the ruffled border geometry of a migratory phagocytic cell. The ruffled border of migratory phagocytic cells on surfaces is known to contain secretory vesicles that release reaction species capable of attacking the alloy.

Corrosion damage by inflammatory cells is further confirmed using SEM imaging methods (see Fig. 5). Direct cellular attack by several different cells can be seen (Fig. 5A) where individual cells create features which are highly self-similar. Each individual cell-attacked

region has a gray mottled or ruffled pattern (Fig. 5A) with a central crater-like pit. An example of single cell attack is shown in both secondary and backscattered imaging (Fig. 5B and 5C). Fine, biologically defined features of the corrosion attack associated with the ruffled border and secretory vesicles, and their relationship to the underlying microstructure can be seen. For example, carbides can be clearly seen in the backscattered images (Fig 5C) as can the fine scale corrosion attack. In the secondary images (Fig. 5B), the corrosion attack topography is altered in the carbide regions, but is still present.

3.2. Evidence of ICI Corrosion on Machined Surfaces Away from the Bearing Surface

There were numerous locations (Fig. 6), on the non-articulating machined surfaces of the CoCrMo components that also showed evidence of ICI corrosion. Figure 6 is a DOM micrograph of the machined surfaces adjacent to the modular taper bore on the head of a MOM CoCrMo component. Patterns of corrosion overlay the machining lines and show similar circular and ruffled characteristics to those corrosion patterns seen in earlier examples on the articular surfaces.

3.3. Evidence of Cellular Remnants and Biological Materials on CoCrMo Surfaces

Cellular remnants and biological materials in morphologies and dimensions suggestive of cells were seen to have been retained relatively intact on some CoCrMo components (see Fig. 7). Figure 7A is a low magnification SEI image of a cluster of such cell remnants and/or biological material in the head articular surface (in the non-contact region). Figure 7B is a high magnification high kV SEI of one such cellular remnant in this cluster. Figures 7C and 7D are low and high kV SEI, respectively, of a cluster of cell remnants showing the contrast differences when the different imaging modes are used confirming that bright regions under low kV reflect cellular and/or biological materials.

3.4. The Role of Fenton Reactions and Reactive Oxygen Species on Corrosion of CoCrMo

Evidence of Fenton reactions comes from the presence of iron nodules that form during the cellular attack. Iron nodules, verified by EDS, not associated with CoCrMo alloys, are consistently observed (see Fig. 8A and 8B) in ICI corroded regions. Numerous examples of iron rich regions associated with streaks from migrating cells contain these iron-rich regions.

3.5. In Vitro testing to simulate ROS interactions with CoCrMo

Open Circuit Potential (OCP) measurements, polarization tests, and electrochemical impedance spectroscopy of Co-Cr-Mo in phosphate buffered saline (pH 7.4 at room temperature) with small additions of hydrogen peroxide between 100 μM and 30 mM, and additions of HCl to adjust pH to as low as 1 were carried out. The results of OCP and polarization tests (Fig. 9A and 9B) show large increases in the corrosion susceptibility of CoCrMo when PBS or PBS with HCl (pH 1 or 3) are modified with small additions of hydrogen peroxide to the solution. OCP (Fig. 9A) becomes significantly more positive (oxidizing) with additions of H_2O_2 and pH 3 PBS can bring the potential of the alloy well into the 0.65 V (vs Ag/AgCl) range. These results were consistent across all samples tested in a particular test. The polarization behavior (V vs Log i, Fig. 9B) also show that the surface of CoCrMo becomes much more susceptible to corrosion attack with H_2O_2 present,

with the corrosion current densities rising over 40 times from the PBS only case, and the zero current potential (corrosion potential) jumps to 0.2 V vs Ag/AgCl. These results support our hypothesis that CoCrMo surfaces corrode when exposed to physiologically representative solutions with small additions of hydrogen peroxide.

3.6. Impedance of CoCrMo in PBS with small additions of H_2O_2

To better understand the effects of H_2O_2 on the corrosion behavior of CoCrMo, the electrochemical impedance spectroscopy (EIS) of this alloy was evaluated in a range of H_2O_2 containing PBS solutions at room temperature. The results, Fig. 10A and 10B, show a large drop in low-frequency impedance (0.01 Hz, associated with the oxide resistance, based on a Randle's circuit approximation of the interface[26]) and narrowing of the frequency range of the phase angle, with small additions of H_2O_2. Even with 0.1 mM H_2O_2, the low-frequency impedance of the surfaces decreases and was about 100 times less when 30 mM H_2O_2 was added to the PBS compared to PBS alone. This shows that H_2O_2 additions to PBS can significantly increase the corrosion susceptibility of CoCrMo alloys, independently from pH.

4. DISCUSSION

This study has provided evidence of direct ICI corrosion attack of CoCrMo in vivo on different implants (hip and knee), with different bearing couples (MOM vs MOP), and on a range of microstructures (cast vs wrought). These observations show that the attack of CoCrMo in the body described here is not limited to any specific design, alloy microstructure or material bearing couple.

The patterns of corrosion on CoCrMo implants, and the intimate association of biological materials with the corrosion show that direct cell attack is taking place. There are different specific patterns of corrosion seen which implies that different cell types, or cell activities are being stimulated. Examples of cells migrating and corroding the surface, leaving behind a streak of corrosion attack rich in iron, shows that Fenton-like reactions are taking place. Other corrosion topographies appear to show individual cells sealing their membrane down on the surface, corroding the surface and leaving behind a fine biological pattern of attack that appears similar to the ruffled border associated with osteoclast resorption. This pattern reflects the local structure of the cell membrane in the perimeter, where sealing occurs, and under the cell where the ruffled border and vesicles assemble to release the oxidizing molecules. The size of attacking cells, based on the corroded regions, is seen to be between 20 μm and 300 μm, although there is evidence of larger foreign body giant cells possibly active as well.

The morphology of the corrosion patterns is consistent with what has been seen previously by Cadosch et al., when inflammatory cells (osteoclasts) corrode stainless steel and titanium alloys in vitro[18,19]. Previous work on activated polymorphonuclear leucocytes on hydroxyapatite biomaterials surfaces also show cellular structures that are highly similar to the morphology of the corrosion patterns reported[20].

The pattern of corrosion under a single cell shows local heterogeneity of the process that is likely the combined effects of the geometry of the ruffled border membrane, the pattern of vesicle deployment, local alloy microstructure and the local constituents released by secretory vesicles. Additionally, the fact that moving inflammatory cells have been observed would imply that these cells are attracted to some stimuli or chemotactic agent, and can remain viable as they attack the CoCrMo and generate ions. The time required to create these patterns of attack is not known at present.

In many cases, cellular remnants and/or biological materials were entwined with the corrosion pits and corrosion patterns demonstrating the interactions between the corrosion and cells. The low kV SEI imaging methods used were an excellent means to distinguish biological materials from the alloy or other features on the metallic surface.

Inflammatory cells are known to use both acid and reactive oxygen species (ROS) secretion to attack invading bacteria and foreign bodies. Osteoclasts, for example, use acid release and ROS[21,22] to attack the mineral (and organic) constituents in bone. The retrieval evidence demonstrates that once activated, inflammatory cells migrate onto and across CoCrMo implants and then attach and seal down on the surface and release the chemical species under their cell membranes between cell and metal (and perhaps into the general solution) to drive the corrosion. A major driver of this attack is reactive oxygen species and their byproducts. In fact, a Fenton reaction[21,23,24] is known to be present in these cell ruffled-border regions. Additionally, the release of transition metal ions like Co^{2+} and Cr^{3+} by the corrosion processes may further assist in the Fenton reactions as these transition metal cations are known to facilitate them[21,23].

One observation made in this study is the presence of metallic iron in multiple sites on the retrieved components in regions undergoing extensive corrosive attack by the cells. CoCrMo alloy does not have significant quantities of iron (less than 0.75 wt%) and it is not discretely distributed on the surface but in solid solution throughout the alloy. Iron is, however, known to play an important role in inflammation of joints[26]. In fact, iron is known to further aggravate inflammation in the presence of reactive oxygen species[27], and to be a central component of the mononuclear phagocyte system (macrophages, osteoclasts, etc.). In rheumatoid arthritis, for example, patients may become anaemic but their inflamed joints or synovial tissues have iron deposits sufficient to stain the tissue[28,29]. Ferritin, a protein known to complex with iron, can sequester approximately 4500 atoms of iron per molecule[30]. Cells use ferritin to maintain iron homeostasis such that it can release iron when levels drop and sequester iron by complexing with excess iron when levels are elevated. In other words, hemorrhages from lesions in the synovial membrane can result in accumulation of blood in the joint. Lysis of erythrocytes in the articular joint will lead to accumulation of iron in the joint in the form of ferritin which are taken up by the macrophages in the synovial membrane as they have a high affinity for iron. Superoxide ($O_2^{-\cdot}$) secreted by activated phagocytes in inflamed synovial tissues can reduce iron bound to ferritin[31]. The reduced iron (via fenton reaction) consequently can act as a catalyst in which ROS intermediates such as superoxide and hydrogen peroxide react to form extremely reactive hydroxyl radical which can cause damage to the adjoining tissue and also may influence the electrochemical behavior of CoCrMo.

It is not clear what process (or condition) is sufficient to induce an activated inflammatory or immune response leading to ICI corrosion. The activation stimuli may be tribocorrosion at bearing surfaces, at modular tapers or other regions, particle generation from UHMWPE, infection, or other unknown patient-specific factors.

Prior studies have shown that so-called biocorrosion can be induced in vitro[18,19] when activated inflammatory cells are cultured directly on stainless steel or titanium. In addition, the patterns of corrosion attack shown in this report are highly similar to the patterns seen when osteoclasts or other phagocytes attack calcium phosphate biomaterials[25] and the cellular structures of polymorphonuclear cells and/or osteoclasts seen in these studies are morphologically similar to the corrosion patterns observed here. This study is the first to present evidence of such attack in-vivo on CoCrMo and it raises several significant questions.

First, what are the conditions necessary for direct cell attack of CoCrMo surfaces to take place in vivo? How pervasive is this observation in implants? A significant majority (51 of 69 components) had documented evidence of ICI corrosion patterns. Whether this rate is reflective of the general population or not is unknown. All components were revised for surgeon identified reasons (Table 1), but, since these observations were serendipitous, it is not possible to assess any causal link between the presence of ICI corrosion and the reason for revision or to determine the incidence of this form of corrosion attack in the general patient population.

Second, how does this observation change the prevailing theories associated with ALTR in joint replacements? It is not clear what role this mode of attack may play, however, if cells are able to directly corrode the implant, then it is likely that as the severity of direct ICI attack increases, larger amounts of ions will be released into the joint space, which may then increase the stimulatory effects on the local biological response. This positive feedback process may lead to continued biological reactions that are self-sustaining regardless of other damage modes present.

Third, the strong oxidizing effects of H_2O_2 and acid between cell membranes and the alloy may create local voltages across CoCrMo surfaces sufficient to result in highly oxidizing conditions. The transpassive potential for CoCrMo in PBS solutions has been reported to be in the 0.5 V vs Ag/AgCl region. Results reported here show that additions of H_2O_2 can raise the corrosion potential up into this region of voltage. These results show that the OCP of CoCrMo may become very positive in vivo and may provide a biological mechanism by which such oxidizing events are possible. It is not known what valence state the surface ions attain when these conditions are present, however, it is generally understood that transpassive corrosion of CoCrMo results in chromium oxide (normally Cr_2O_3 oxide film) oxidizing further to lose passivity[20].

The in vitro corrosion studies demonstrate that small additions of H_2O_2 can increase the corrosion susceptibility of CoCrMo. If the joint fluid can accumulate sufficient quantities of reactive oxygen species, then similar effects may arise not only under the cells themselves but in the general joint fluid surrounding the implant. How much ROS is contained in

inflamed joint fluids is not known, but should be investigated. These fluid changes may also alter processes of corrosion for CoCrMo in regions like bearing surfaces as well as within modular taper crevices as the ROS-containing fluid penetrates into the crevice.

There are several limitations of this study. The initial observation of ICI corrosion was found incidentally during retrieval studies focused on modular taper corrosion. The high number of components with ICI corrosion may be a consequence of this focus but this cannot be determined in this cohort of implants. The evidence presented has not captured the direct interaction of a cell and the corrosion pattern as the implants were cleaned and sterilized during handling. Future studies are planned to try to preserve the interacting biological structures and the alloy surface to show this linkage and to develop in vitro cell metal tests to show this effect.

The patterns shown, much like fatigue striations in a fatigue fracture sample, are forensic evidence for the processes described. These patterns occurred on machined surfaces, where no tribological processes are present, as well as on articulating surfaces that were not involved in contact or wear and thus these are not, and do not appear to be of a tribocorrosion origin. The fine submicron scale patterns of corrosion seen across numerous implants, alloy types and bearing combination are highly consistent and cannot be explained by other corrosion processes or other aspects of the implant body system.

Whether this is a new phenomenon, or something that has been occurring for decades, but has been missed by the research community is unknown at this time.

The time-dependent level of ROS generation possible under activated cells on CoCrMo is not known. Thus, whether or not the levels of H_2O_2 tested in vitro to cause corrosion susceptibility changes may or may not be reflective of in vivo conditions.

5. Conclusions

In summary, evidence of direct in vivo inflammatory cell induced corrosion of CoCrMo alloy has been documented for the first time on retrieved hip and knee implants. The cellular attack left patterns of corrosion damage and remnant biological materials and/or cellular debris on both articulating and non-articulating (machined) implant surfaces not engaged in tribocorrosion processes. The corrosion patterns left on CoCrMo surfaces were highly reflective of the cellular structures causing the damage and included evidence of cell migration and corrosion by way of Fenton-like reactions. The presence of inflammatory cell induced corrosion was independent of the counter bearing surface materials being seen in both MOM implants and MOP devices. The metallurgy of the CoCrMo did not limit the corrosion as both cast and wrought alloys were seen to be attacked. Hydrogen peroxide and HCl, known reactive species in inflammatory cells, induce significantly increased OCP and increased corrosion rates of CoCrMo in vitro at relatively low concentrations. These chemicals are similar to what is expected to occur under phagocytic cells during activation and attack and demonstrate at least part of the mechanism of inflammatory cell induced corrosion.

Acknowledgments

Support for this work was provided, in part, by Depuy Synthes, and NIH R01 AR47904 (NIAMS). We are grateful to the surgeons and Implant retrieval centers that provided the implants for analysis.

Disclosures: JLG currently receives grant funding from corporate sources including Stryker Orthopedics and Depuy Synthes. He is a consultant for Medtronic, Stryker Orthopedics, Biomet and Depuy Synthes. JLG is also Editor-in-Chief of the Journal of Biomedical Materials Research - Part B: Applied Biomaterials.

The institutions of SMK currently receive support from the NIH R01 AR47904, as well as from Stryker Orthopedics, Zimmer, Biomet, Depuy Synthes, Smith and Nephew, Medtronic, Invibio, Stelkast, Ticona, Formae, Kyocera Medical, Wright Medical Technology, Ceramtec, and DJO. He is on the editorial board of the Journal of Arthroplasty.

References

1. F-75, Annual Book of Standards. Vol. Vol 13. American Society for Testing and Materals, ASTM International; 1996. Standard Specification for Cobalt- 28 Chromium – 6 Molybdenum castings and casting alloy for surgical implants.
2. F-1537, Annual Book of Standards. Vol. Vol 13. American Society for Testing and Materials, ASTM International; 1996. Standard Specification for Wrought Cobalt – 28 Chromium – 6 Molybdenum Alloy for Surgical Implants.
3. Cook RB, Bolland JRF, Wharton JA, Tilley S, Latham JM, Wood RJK. Pseudotumor formation due to tribocorrosion at the taper interface of large diameter metal on polymer modular total hip replacements. J Arthroplasty. 2013; 28:1430–1436. [PubMed: 23528556]
4. Kwon YM, Ostlere SJ, McLardy-Smith P, Athanasou NA, Gill HS, Muray DW. Asymptomatic pseudotumors after metal-on-metal hip resurfacing arthroplasty: prevalence and metal ion study. J Arthorplasty. 2011; Vol 26(#4):511–518.
5. Langton DJ, Joyce TJ, Jameson SS, Lord J, Van Orsouw M, Holland JP, Nargol AVF, De Smet KA. Adverse reaction to metal debris following hip resurfacing: the influence of component type, orientation and volumetric wear. J Bone Joint Surg, Br. 2011; Vol. 93(No 2):164–171. [PubMed: 21282753]
6. Natu S, Sidaginamale RP, Gandhi J, Langton DJ, Nargol DJ, Antoni VF. Adverse reactions to metal debris: histopathological features of periprosthetic soft tissue reactions seen in association with failed metal on metal hip arthroplasties. J Clinic Path. 2012; Vol 65(No 5):409–418.
7. Fricka KB, Ho H, Peace WJ, Engh CA. Metal-on-metal local tissue reaction is associated with corrosion of the head taper junction. J Arthoplasty. 2012; Vol 27 Suppl1(No 8):26–31.
8. Jacobs JJ, Urban RM, Hallab NJ, Skipor AK, Fischer A, Wimmer MA. Metal-on-metal bearings. J Amer Acad Orthop Surg. 2009; Vol 17(No 2):69–76. [PubMed: 19202120]
9. Gilbert JL, Buckley CA, Jacobs JJ. In-vivo corrosion of modular hip prostheses in mixed and similar metal combinations: The effect of stress, motion and alloy coupling. J Biomed Mat Res. 1993; 27(12):1533–1544.
10. Jacobs JJ, Gilbert JL, Urban RM. Current concepts review: Corrosion of metal orthopaedic implants. J Bone Joint Surg. 1998; 80-A(2):268–282. [PubMed: 9486734]
11. Yan Y, Neville A, Dowson D. Tribocorrosion properties of cobalt-based medical implant alloys in simulated biological environments. Wear. 2007; 263:1105–1111.
12. Gilbert, JL. ASM International Handbook. Vol. Vol. 13C. Materials Park, OH: Corrosion; 2006. Mechanically assisted corrosion of metallic biomaterials; p. 826-836.
13. Cooper HJ, Della Valle CJ, Berger RA, Tetreauly M, Paprosky WG, Sporer SM, Jacobs JJ. Corrosion at the head-neck taper as a cause for adverse local tissue reactions after total hip arthroplasty. J Bone Joint Surg. 2012 Sep; Vol 94A(Issue 18):1655–1661. [PubMed: 23289127]
14. Gill IPS, Webb J, Sloan Beaver RJ. Corrosion at the neck-stem junction as a cause of metal ion release and pseudotumor formation. J Bone Joint Surg Br. 2012; Vol 94B(No 7):895–900. [PubMed: 22733942]

15. Lindgren JU, Brismar BH, Wikstron AC. Adverse reaction to metal release from a modular metal-on-polyethylenee hip prosthesis. J Bone Joint Surg Br. 2011; Vol 93(No 10):1427–1430. [PubMed: 21969447]

16. Hallab NJ, Jacobs JJ. Biological Effects of implant debris. Bulletin of the NYU hospital for joint diseases. 2009; Vol 67(No 2):182–188. [PubMed: 19583551]

17. Jacobs JJ, Hallab NJ, Urban RM, Wimmer MA. Wear particles. J Bone Joint Surg. 2006; Vol 88(suppl 2):99–102. [PubMed: 16595453]

18. Cadosh D, Chan E, Gautischi OP, Simmen HP, Filgueira L. Bio-Corrosion of stainless steel by osteoclasts – In Vitro Evidence. J Orthop Res. 2009; 27:841–846. [PubMed: 19105228]

19. Cadosh D, Al-Mushaiqri MS, Gautischi OP, Meagher J, Simmen HP, Filgueira L. Bio-Corrsion and uptake of titanium by human osteoclasts. J Biomed Mat Res – A. 2010; 95A:1004–1010.

20. Velard F, Braux J, Amedee J, Laquerriere P. Inflammatory cell response to calcium phosphate biomaterial particles. Acta Biomat. 2013; 9:4956–4963.

21. Rosen GM, Pou S, Ramos CL, Cohen MS, Britigan BE. Free radicals and phagocytic cells. The FASEB Journal. 1995; 9:200–209.

22. Laskin DL, Pendino KJ. Macrophages and inflammatory mediators in Tissue injury. Annu Rev Pharmacol Toxicol. 1995; 35:665–677.

23. Prousek J. Fenton chemistry in biology and medicine. Pure Appl Chem. 2007; Vol 79(No 12): 2325–2338.

24. Pourbaix, M. Atlas of electrochemical equilibria in aqueous solutions. NY: Pergamon Press; 1966. p. 264

25. Schilling AF, Linhart W, Filke S, Gebauer M, Shinke T, Rueger JM, Amling. Resorbability of bone substitute biomaterials by human osteoclasts. Biomaterials. 2004; 25:3963–3972. [PubMed: 15046886]

26. Alya, J Dabbagh; Charles, W Trenam; Chris, J Morris; David, R Blake. Iron in joint inflammation. Annals of the Rheumatic Diseases. 1993; 52:67–73. [PubMed: 8427520]

27. Christopher, J Morris; John, R. Earl; Charles, W Tream; David, R Blake. Reactive Oxygen Species and Iron- a Dangerous Partnership in Inflammation. International Journal of Biochemistry and Cell Biology. 1995; 27(2):109–122. [PubMed: 7767779]

28. Weber J, Julius HW, Verhoef CW, Were JM. Were, Absorption and Retention of Iron in Rheumatoid Arthritis. Annals of the Rheumatic Diseases. 1973; 32:83. [PubMed: 4685885]

29. Goris, Roosendaal; Marieke, E Vianen; Marion, JG Wenting; Cornelis van Rinsum, A.; Marijke van den Berg, H.; Floris, PJG Lafeber; Johannes, WJ Bijlsma. Iron deposits and catabolic properties of synovial tissue from patients with haemophilia. The Journal Of Bone And Joint Surgery. 1998; 80-B(3):540–545.

30. Biemond P, Swaak AJ, van Eijk HG, Koster JF. Intraarticular ferritin-bound iron in rheumatoid arthritis. A factor that increases oxygen free radical-induced tissue destruction. Arthritis and Rheumatism. 1986; 29(10):1187–1193. [PubMed: 3768055]

31. Lunn JV, Gallagher PM, Hegarty S, Kaliszer M, Crowe J, Murray P, Bouchier-Hayes D. Bouchier-Hayes, The role of hereditary hemochromatosis in aseptic loosening following primary total hip arthroplasty. Journal of Orthopaedic Research. 2005; 23:542–548. [PubMed: 15885473]

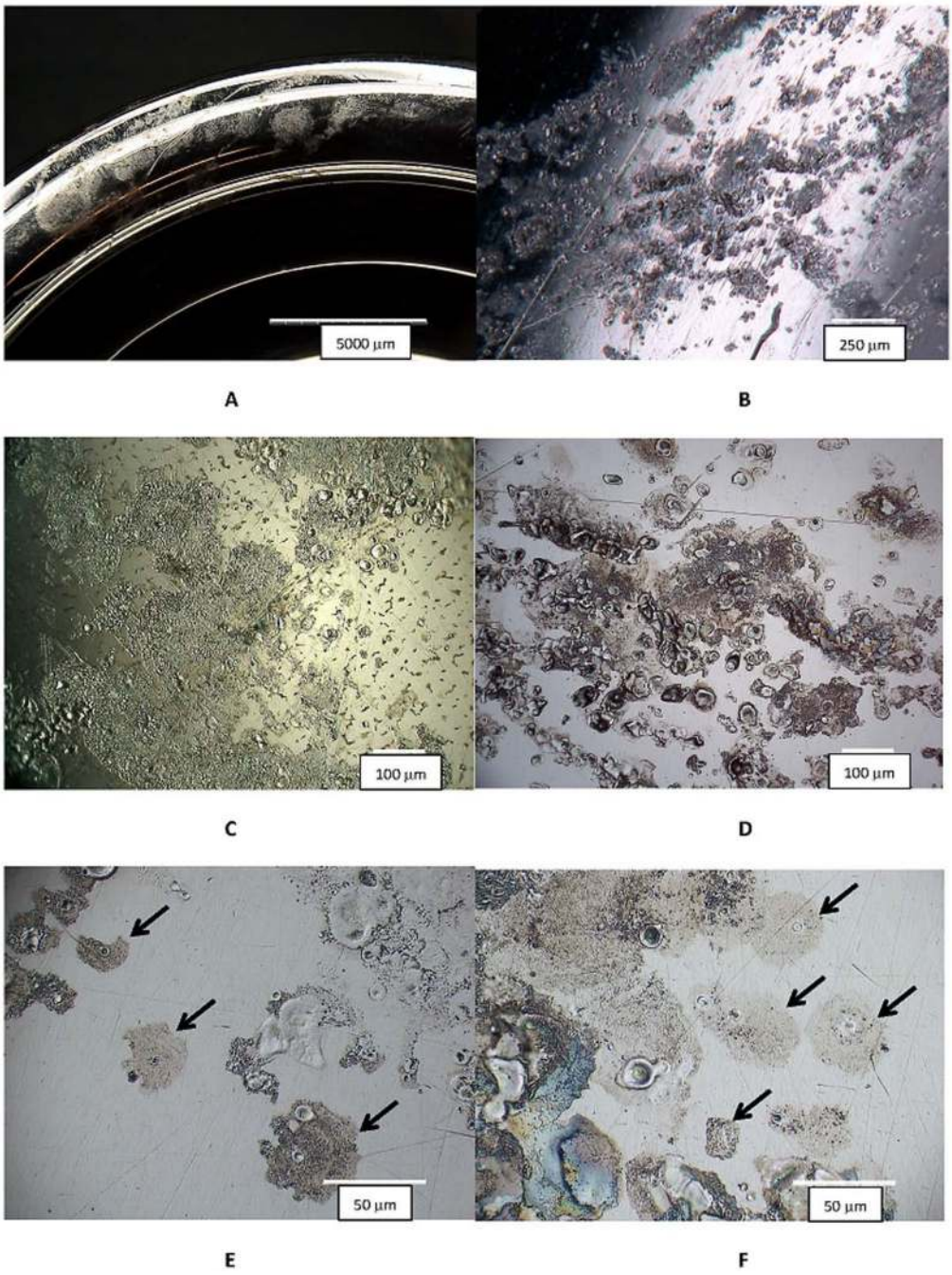

Figure 1.

Digital optical micrographs (DOM) of different retrieved CoCrMo hip implants with evidence of inflammatory cell induced (ICI) corrosion. Implants were hips and knees and both metal-on-polyethylene (MOP) and metal-on-metal (MOM) devices, with different metallurgical conditions (wrought and cast). A) low magnification DOM image of the rim of a metal acetabular liner component with a frosted appearance that is visual evidence of ICI corrosion (Bar = 5 mm). B) A higher magnification image of the head bearing region of a MOP couple showing multiple spots of ICI corrosion (bar = 250 µm). C) An optical

micrograph from a knee implant (cast CoCrMo and MOP bearing) showing the nature of the corrosion attack resulting from inflammatory cells. This attack was located on the posterior condular surface of the femoral component (bar = 100 μm). D) DOM image of a MOM head with ICI corrosion patterns. E) Higher magnification DOM image of the head in D showing isolated cell attack regions (Arrows). F) Higher magnification DOM image of the MOP head in B with specific cell-attack regions (Arrows). There are several common features in these images. First, patterns are all on the 10 to 100 um length scale consistent with cellular dimensions and individual cell corrosion spots (see arrows in 1E and 1F) which have a central flat smooth oval or circular crater-like spots surrounded by a frosted pattern of ruffled topography. Some images show single roughly circular spots of attack while other regions appear to result from either larger single cells, multiple cells or single-moving cells attacking the CoCrMo surface.

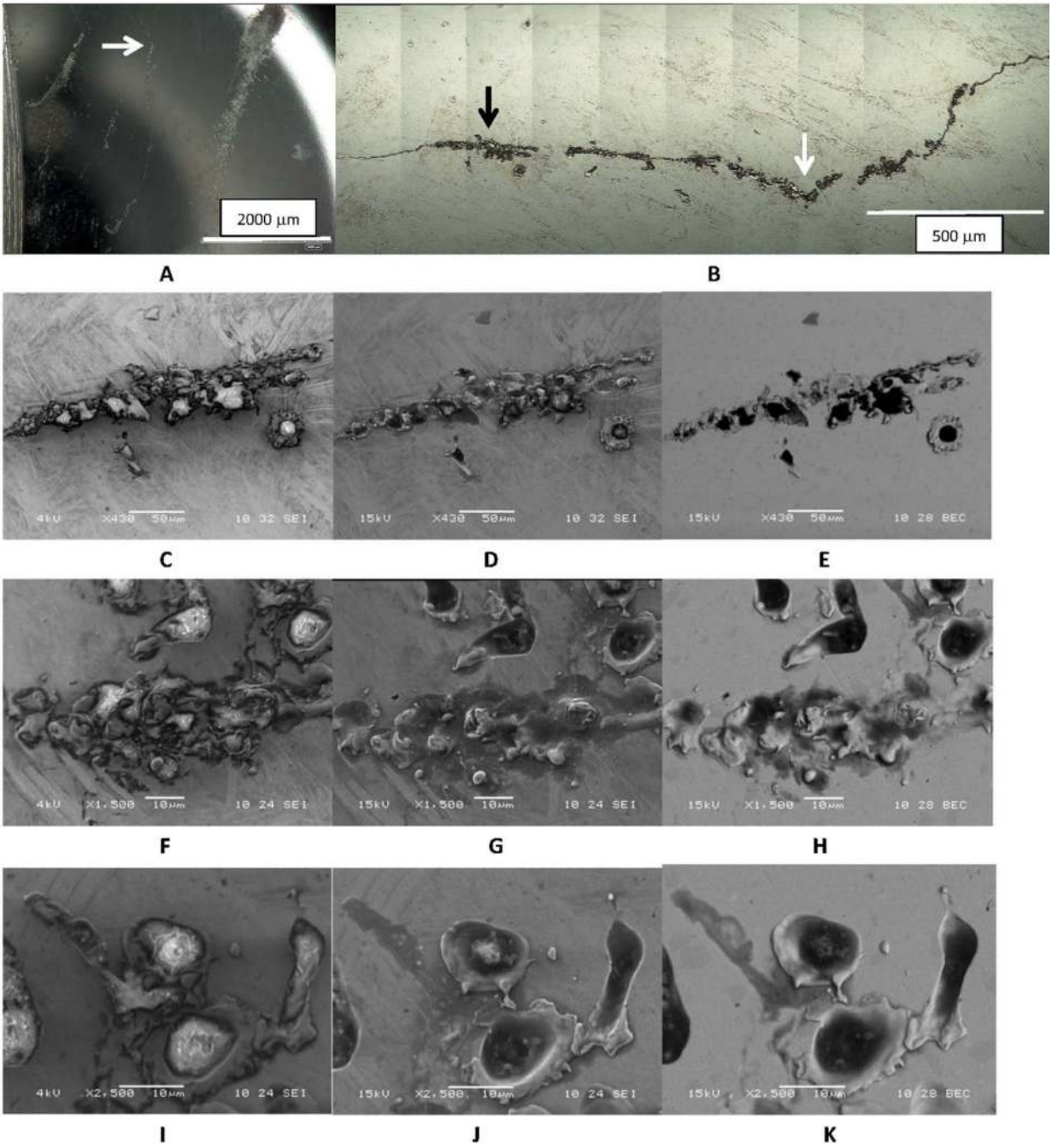

Figure 2.

Series of DOM images of a CoCrMo head bearing surface in a non-contact region showing a line of corrosion suggestive of a transiting cell. A) Low magnification optical micrograph of the region. The line of corrosion runs vertically in the center and there is surrounding cell-induced corrosion present. B) Digital Optical Montage of line of corrosion in 2A (White arrow corresponds to location in 2A and black arrow corresponds to images in C-E). C-E) Low magnification SEM micrographs at C) low kV SEI, D) high kV SEI and E) high kV BEC. F-H is an intermediate magnification set of micrographs while I-K is a higher

magnification set of SEM micrographs under each voltage condition of another location along the line of corrosion. The low kV images all reveal remnant biological material in the corroded regions, while the high kV SEI and BEC images show the underlying metal and the corrosion patterns. The corrosion is not tribological in appearance but shows a migrating cell attack and remnant biological materials and/or remnant cells in the corroded regions as can be seen in comparison of the low kV and high kV images.

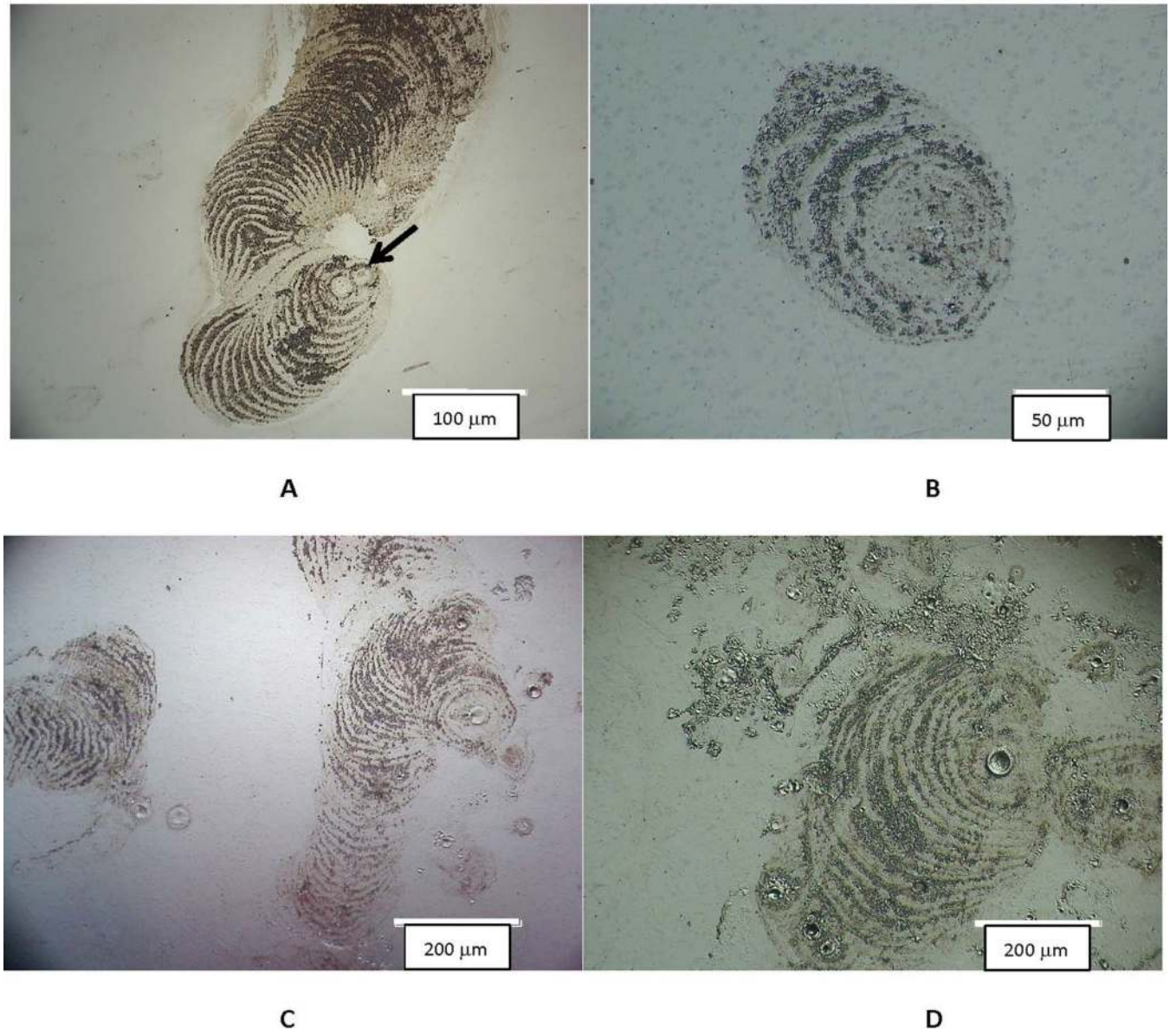

Figure 3.

DOM images of different implant articulating surface with patterns of cell attack where individual cells moved while corroding the surface. These concentric ring-like patterns show that these inflammatory cells attach to and migrate on the Co-Cr-Mo surface. They attach to, spread and migrate on, and attack the surface in a way that is consistent with how adherent osteoclasts, for example, attack bone or hydroxyl apatite[25]. A) Head of a hip implant in a MOP bearing (bar = 100 μm). Note that in this example the cellular attack appears to start in the lower middle of the micrograph, begins to migrate to the left and down, and then turns and begins to advance upward. Each concentric ring is where the cell has attacked the substrate and then advanced to the next front (smooth region) and attacked the next layer, repeating the process. B) to D) Are additional examples from MOM heads (bar = 200 μm). Note the consistency in the attack across implants.

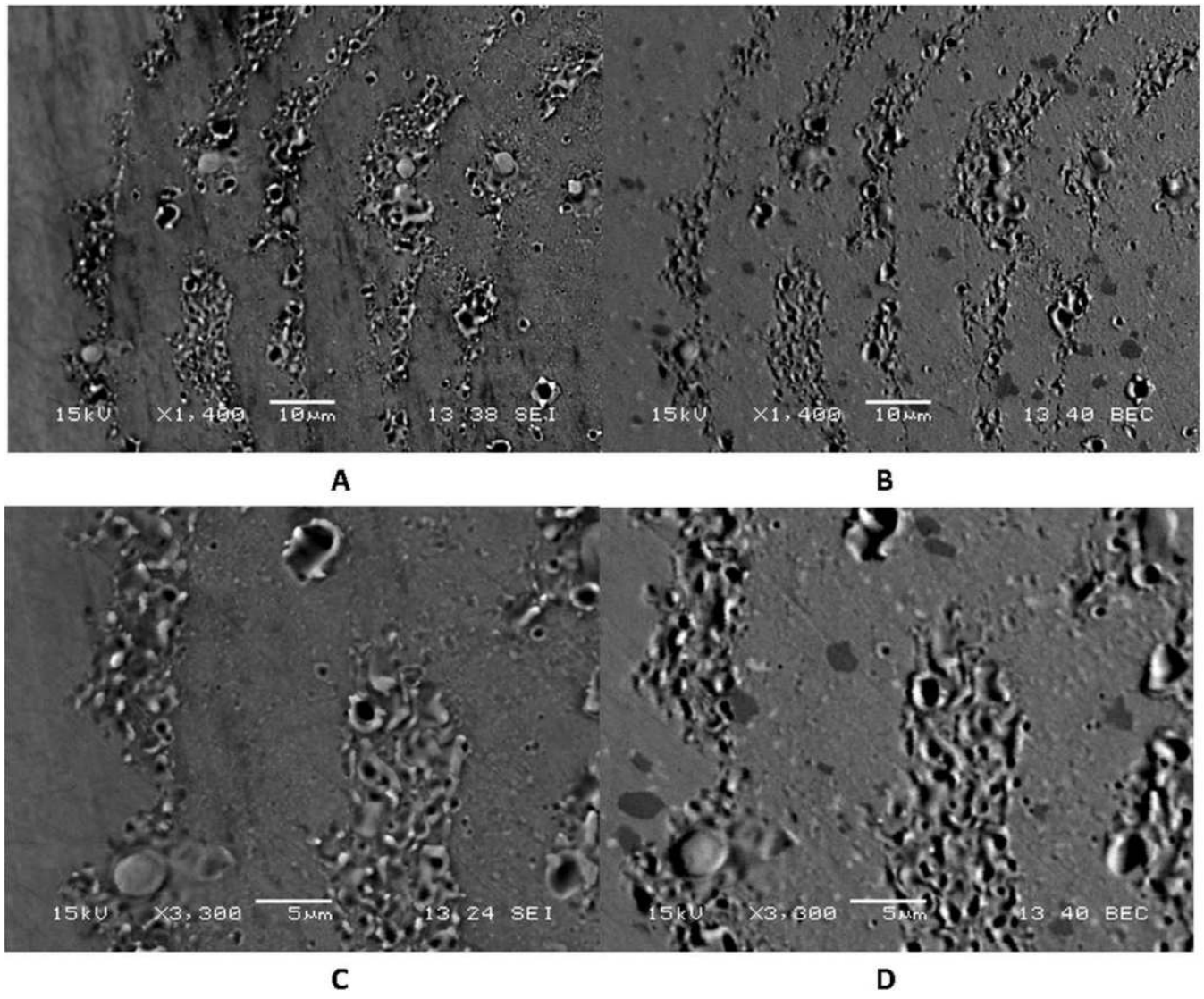

Figure 4.

SEM micrograph pairs showing details of corrosion patterns described in Fig. 3. A) SEI and B) BEC images of the same region showing the concentric rings of corrosion. C) SEI and D) BEC images under higher magnificent of the same regions. Note the fine biologically-driven corrosion patterns as well as the underlying microstructure of the CoCrMo alloy exhibiting carbides and other features of the microstructure and its interaction with the ICI corrosion.

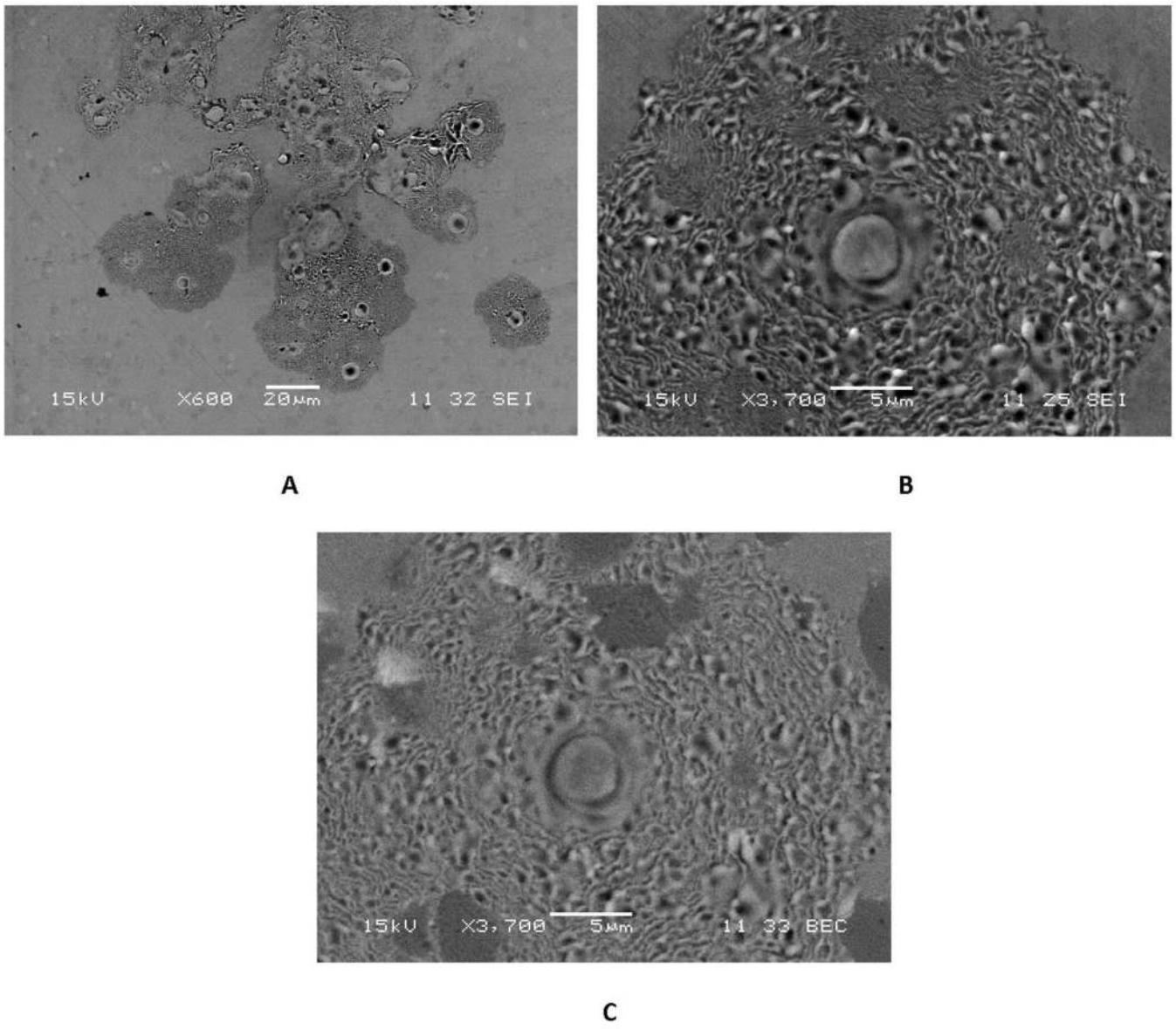

Figure 5.

SEM micrograph showing examples of A) groups, and B) and C) individual ICI corrosion patterns. A) A small collection of relatively stationary cells attacking a CoCrMo surface. B) and C) are secondary and backscattered electron pairs documenting the fine detail of an individual inflammatory-cell-induced corrosion damage site. The fine detailed pattern of the ruffled border morphology is reflected in the corrosion damage and the regions where carbides and oxides are present there is a diminished extent of attack, but still the fine ruffled features are present even on the carbides.

Figure 6.
Digital optical micrograph of a CoCrMo head where ICI corrosion has taken place on a non-articulating machined surface adjacent to the modular taper bore. Machining lines are damaged by the ICI corrosion process in patterns consistent with the ICI corrosion seen in earlier examples on articular surfaces. The modular taper bore is about 3 mm to the lower right.

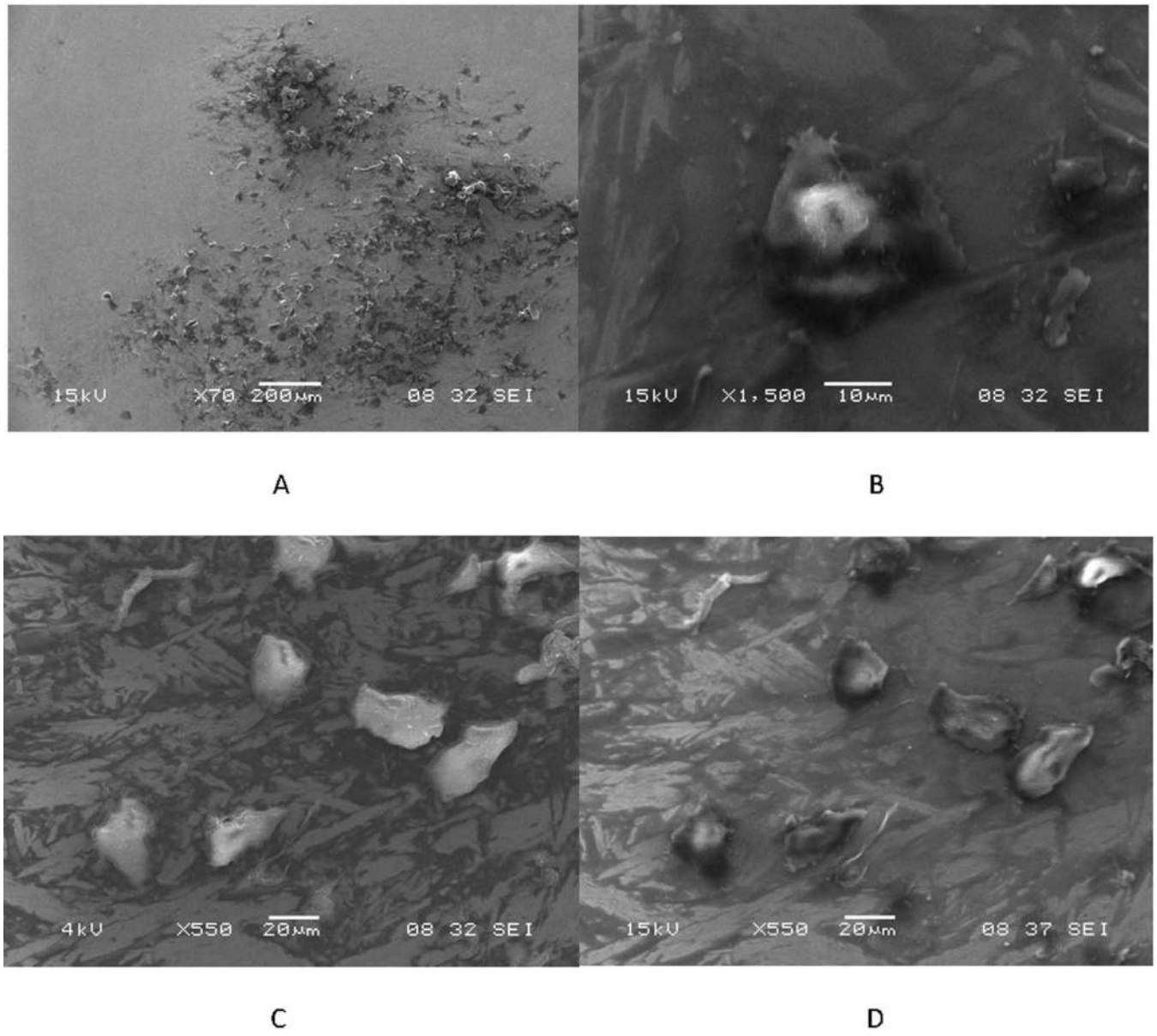

Figure 7.

Scanning electron micrographs of a region of a MOM head that had a cluster of adherent cellular debris. A) Low magnification SEI of the cell cluster. B) higher magnification, high kV SEI of an individual cell in this cluster. C) and D) low kV SEI and high kV SEI of the same grouping of cells. Note the bright contrast for the cells in (C) highlighting the cellular material.

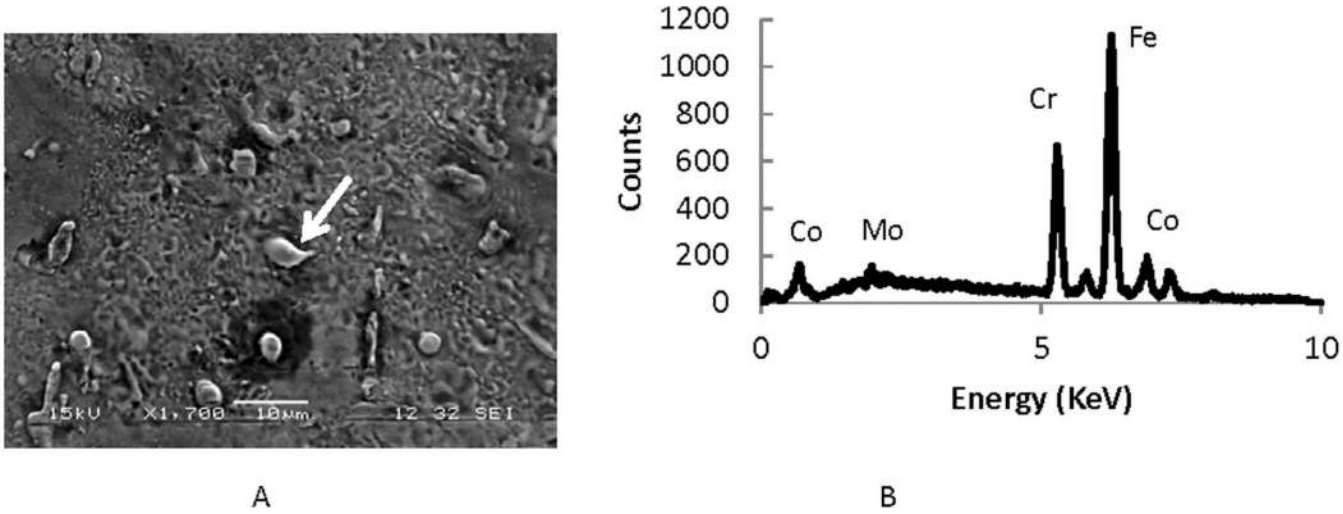

Figure 8.

Evidence of a Fenton-like reaction during ICI corrosion. A) SEI of ICI corroded region in which there is an Fe-rich particle (white arrow)). B) EDS spectrum confirming the presence of Fe in that location and a decrease in cobalt. The nodules in this cell-corroded region are high in iron implying that a Fenton-like reaction was involved in the corrosion of CoCrMo alloy. This finding of nodules rich in iron was seen in most of the cell-induced corrosion regions analyzed and in the streaks (Fig. 2) associated with migrating cells.

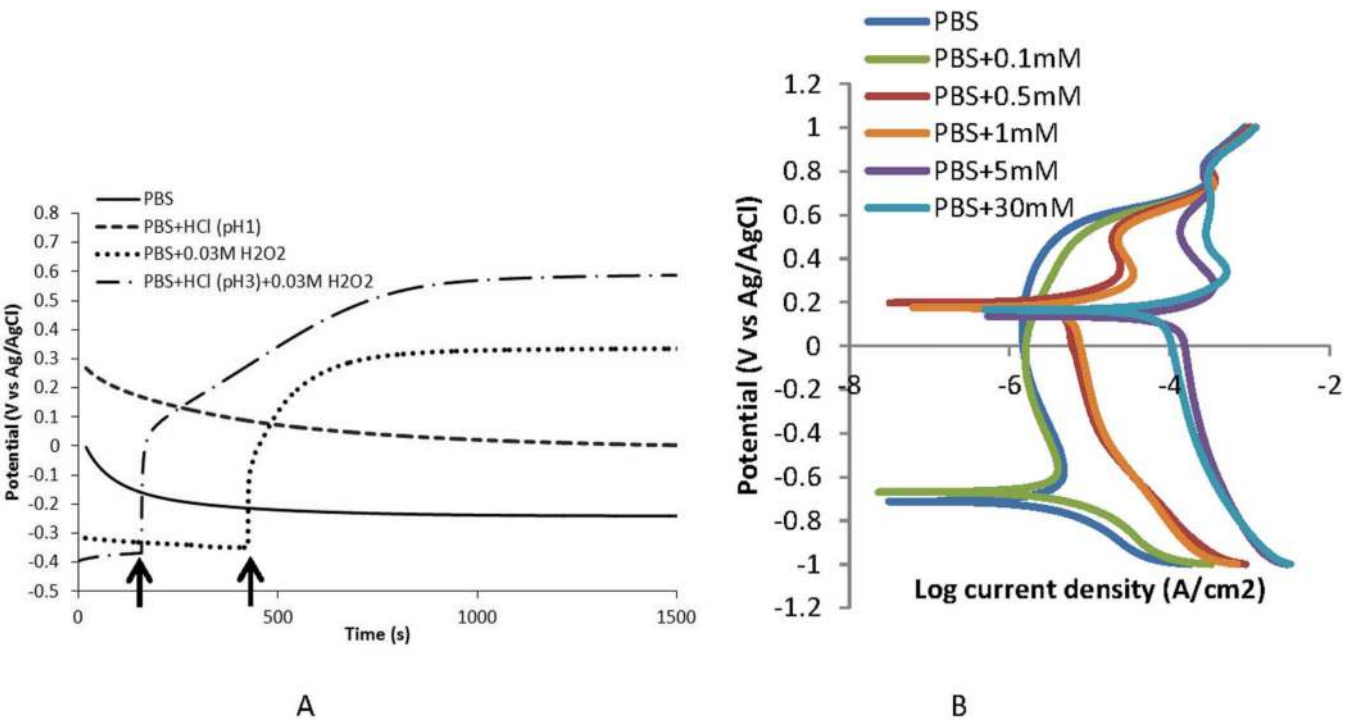

Figure 9.

A) Open circuit potential plots of CoCrMo in phosphate buffered saline (PBS, pH 7.4, room temperature) and in solutions modified with HCl (pH 1 and 3) and H_2O_2 (0.03M). OCP was raised above PBS levels to a higher oxidizing potential when acid alone, or H_2O_2 alone were added to the PBS solution (see arrows). When both acid and H_2O_2 are added to PBS, the OCP rises to above 0.6 V vs Ag/AgCl which is a highly oxidizing condition for CoCrMo. B) Polarization plots of CoCrMo in PBS solutions with differing amount of H_2O_2. As H_2O_2 concentration increases from 0.1 mM to up to 30 mM, the corrosion currents rise significantly above the PBS alone and the corrosion potential shifts positively to 0.2 V.

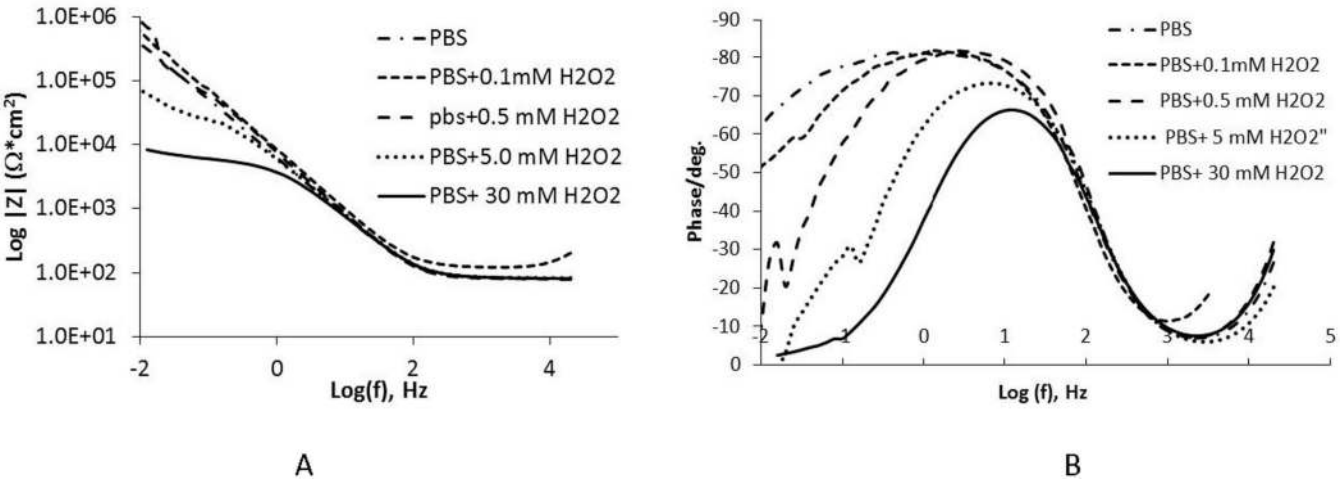

Figure 10.

Impedance analysis results for CoCrMo in PBS containing differing concentations of H_2O_2. A) impedance versus log of the frequency, B) phase angle versus log of the frequency. Note, that small increases in H_2O_2 concentrations in pH 7.4 PBS result in large (two orders of magnitude) decrease in the low frequency impedance, reflective of the oxide resistance, of the surface.

Table 1

Summary of stated reasons for revision associated with MOP hips, MOM hips and knees.

Reasons for Revision	Implant Type		
	MOP Hip (18)	MOM Hip (19)	Knee (14)
Infection	5	1	8
Loosening	13	2	6
ALTR	0	11	0
Pain	1	16	1
Other	1	4	1

Note, several revision reports listed multiple reasons all of which are captured here. The other category includes fracture of the stem, osteolysis, subluxation, avascular necrosis, and mechanical failure (unspecified).